A Multi-Autonomous Underwater Vehicle System for Autonomous Tracking of Marine Life

• •

Yukun Lin

Department of Computer Science and Mathematics, Harvey Mudd College, Claremont, CA 91711
e-mail: ylin@hmc.edu

Jerry Hsiung

Department of Computer Science, Harvey Mudd College, Claremont, CA 91711
e-mail: shsiung@hmc.edu

Richard Piersall

Department of Engineering, Harvey Mudd College, Claremont, CA 91711
e-mail: rpiersall@hmc.edu

Connor White

Department of Biological Sciences, CSU Long Beach, Long Beach, CA 90840
e-mail: connor.white@student.csulb.edu

Christopher G. Lowe

Department of Biological Sciences, CSU Long Beach, Long Beach, CA 90840
e-mail: clowe@csulb.edu

Christopher M. Clark

Department of Engineering, Harvey Mudd College, Claremont, CA 91711
e-mail: clark@hmc.edu

This paper presents a multi-autonomous underwater vehicle system capable of cooperatively and autonomously tracking and following marine targets (i.e., fish) tagged with an acoustic transmitter. The AUVs have been equipped with stereo-hydrophones that receive signals broadcasted by the acoustic transmitter tags to enable real-time calculation of bearing-to-tag and distance-to-tag measurements. These measurements are shared between AUVs via acoustic modem and fused within each AUV's particle filter for estimating the target's position. The AUVs use a leader/follower multi-AUV control system to enable the AUVs to drive toward the estimated target state by following collision-free paths. Once within the local area of the target, the AUVs circumnavigate the target state until it moves to another area. The system builds on previous work by incorporating a new SmartTag package that can be attached to an individual's dorsal fin. The SmartTag houses a full inertial measurement unit (INU), video logger, acoustic transmitter, and timed release mechanism. After real-time AUV tracking experiments, the SmartTag is recovered. Logged IMU data are fused with logged AUV-obtained acoustic tag measurements within a particle filter to improve state estimation accuracy. This improvement is validated through a series of multi-AUV shark and boat tracking experiments conducted at Santa Catalina Island, California. When compared with previous work that did not use the SmartTag package, results demonstrated a decrease in mean position estimation error of 25–75%, tag orientation estimation errors dropped from $80°$ to $30°$, the sensitivity of mean position error with respect to distance to the tag was less by a factor of 50, and the sensitivity of mean position error with respect to acoustic signal reception frequency to the tag was 25 times less. These statistics demonstrate a large improvement in the system's robustness when the SmartTag package is used. © 2016 Wiley Periodicals, Inc.

1. INTRODUCTION

Studying the spatial movement of sharks and other fishes is an important tool for monitoring habitat and maintaining fish populations. Typical methods for tracking fish include tagging individuals with acoustic transmitters, and then using hydrophone-receiver systems to detect and measure the signals transmitted. Often, the hydrophone-receivers are placed at fixed locations around an environment of interest to passively track tagged individuals that move through the

Direct correspondence to: Yukun Lin, e-mail: ylin@hmc.edu

static array (Espinoza, Farrugia, Webber, Smith, & Lowe, 2011). For an increased area of coverage, satellite tags are used but they can only provide positional data when the fish is at the surface.

Alternatively, active tracking can be done manually by mounting a directional hydrophone on a boat and continuously following the tagged individual from the surface for periods up to 96 h (Lowe & Bray, 2006). However, such a method is often labor intensive and can be cost prohibitive. Thus, the development of an autonomous tracking system that can produce high-resolution positional data would provide an essential tool in understanding how changes in environmental conditions influence the behavior of fish.

The authors have demonstrated in Clark et al. (2013) that a single AUV system using low-resolution angle measurements, distance measurements, and depth measurements is able to autonomously track and follow a tagged leopard shark. Key components of the system include a circle tracking controller and state estimator presented in Tang, Shinzaki, Lowe, & Clark (2012) and Lin et al. (2014).

This paper builds on previous works and presents a multi-AUV system capable of tracking and following a tagged leopard shark. Multi-robot systems have demonstrated advantages over single robot systems in that they have greater resolution in spatio-temporal sampling and robustness to noisy sensor measurements. That is, many robots can be located at different locations in the environment to simultaneously obtain sensor measurements of the environment or targets being tracked. This is highly relevant to fish tracking, where acoustic sensors are unreliable (e.g., because of the occlusion with kelp beds, subject to variation in transmission medium characteristics like temperature, multi-path effects on surface/seafloor, etc.), and multiple measurements taken from different sensor vantage points can lead to increased measurement frequency. However, using multiple robots requires robot coordination to ensure the robots (1) don't collide and (2) take advantage of their simultaneous presence. This paper presents a method to coordinate a system of AUVs to leverage their ability to simultaneously detect and sense the sharks being tracked.

The system consists of two OceanServer IVER2 AUVs (Figure 1(a)), each equipped with a Lotek MAP RT stereo-hydrophone system that detects acoustic signals from of-the-shelf Lotek fish tags. The Lotek tags are part of a *Smart-Tag* package (Figure 1(b) and Figure 3) that includes a 9-DOF (degrees of freedom) Loggerhead IMU with a timer based release mechanism. A distributed particle filter is used to estimate the three-dimensional (3D) position of the tagged fish in real time. An autonomous control system is employed that drives the AUVs toward the estimated position of the tagged fish and circles it (Figure 1(c)). This enables the AUVs to maintain a stand-off distance from the tagged fish in order to minimize the influence on its behavior. In developing

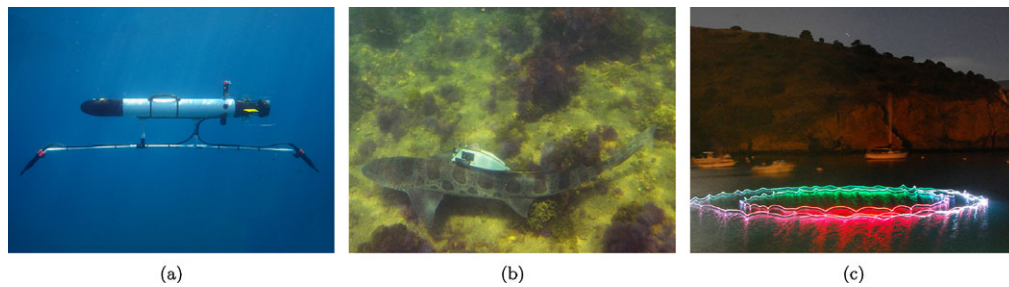this system, several contributions have been made to the field of underwater robotics:

- A decentralized multi-AUV control system that incorporates A* path planning for obstacle avoidance with two modes of target tracking: (1) path-to-target following and (2) target circumnavigation.
- A distributed multi-AUV online state estimator that enables real-time AUV estimation of tagged fish states.
- The design, development, and deployment of a SmartTag package that includes a Lotek fish tag, and a Loggerhead IMU with tri-axis gyroscope, accelerometer, and magnetometer. A timer based burn wire is used to release the tag package.
- An offline state estimator that integrates the IMU data with measurements from the AUV to increase accuracy in position and orientation estimation of the tagged fish.

The paper is organized as follows: Section 2 describes the past work and related research on the topic. Section 3 gives an overview of the multi-AUV system, and Sections 4 and 6 discuss the state estimator and controller, respectively. Sections 6 and 7 present the experiments and results performed with the system. Conclusions and future work are presented in Section 8.

2. BACKGROUND

Tracking stationary and moving targets with robotic systems is a well-studied field of research (Grothues, Dobarro, & Eiler, 2010; Kobilarov, Sukhatme, Hyams, & Batavia, 2006; Montemerlo, Thrun, & Whittaker, 2002; Rife & Rock, 2003; Schulz, Burgard, Fox, & Cramers, 2001, 2003). Within the context of using underwater robots to track individuals, both optical-based methods (Georgiades et al., 2004; Rife & Rock, 2003; Zhou & Clark, 2006), and acoustic-based methods (Grothues et al., 2008; Oliver et al., 2013) have been used. In Rife & Rock (2003), autonomous tracking of jellyfish with a remotely operated vehicle (ROV) was conducted using basic image processing techniques. Work presented in Zhou & Clark (2006) demonstrated the use of SIFT features in tracking individual fish between video frames captured from an ROV. Image processing techniques were also shown to be useful in tracking divers with a robot in Georgiades et al. (2004). Unfortunately, most optical methods employed in underwater environments suffer from limited visibility due to poor lighting conditions and the presence of debris.

While acoustic methods of tracking marine individuals have been used for decades, hydrophone receivers have only recently been mounted on underwater vehicles. For example, work done by Grothues, Dobarro, & Eiler (2010); Grothues et al. (2008) has demonstrated the ability to track tagged sturgeon using a REMUS AUV equipped

Figure 1. Hydrophones mounted on a prototype PVC frame attached to an OceanServer Iver2, suspended 0.4 m down with 2.4 m of separation (a). A leopard shark tagged with the SmartTag package (b). The two AUVs circle in phase around the estimated target position (c). This photo was taken using a long exposure during a night deployment in which the leopard shark remained in shallow water and the AUVs remained at the surface. Different-colored lights mounted on different sides of the AUV masts indicate the AUV yaw angle

with a Lotek hydrophone system. Work in Haulsee et al. (2015) demonstrated how AUVs can be used for determining habitat selection of tagged sand tiger sharks. Unlike the work presented by the authors, work by (Grothues, Dobarro, & Eiler, 2010; Grothues et al., 2008; Haulsee et al., 2015) did not use in situ measurements to actively steer the AUV.

The use of IMU tags on marine animals by itself is also not novel. Traditionally, these tags only have accelerometers and are attached to the fins or tails. The frequency and amplitude of the tail/fin beats as measured by the accelerometers are then used to infer the behavioral state of the animals (Shepard et al., 2008). The use of IMU tags that include magnetometers and gyroscopes is a more recent development (Noda, Kawabata, Arai, Mitamura, & Watanabe, 2014). As well, they have not be been combined with acoustic transmission measurements for tracking marine life.

The authors are also aware of the tracking of a white shark using a REMUS-100 AUV conducted by researchers at the Woods Hole Oceanographic Institute (WHOI). Their work was featured by Discovery Channel in 2013. In their approach, a cylindrical transponder approximately 30 cm long is used as a tag. An ultra-short baseline receiver mounted on the REMUS-100 AUV queries the transponder to determine range and bearing (Packard et al., 2013). Unfortunately, the large size of the transponder greatly limits the use to particularly large marine animals.

Our approach uses smaller off-the-shelf Lotek acoustic tags that are 80 mm long and 16 mm wide. The Lotek tags are capable of only pulse transmissions and are similar to the 10,000 tags already being used, hence making this system easily applicable to existing fish studies. While bearing and range measurements obtained from these tags tend to be less accurate than that of a transponder, the small size of these tags makes them applicable to a large variety of smaller fish. Also unlike Packard et al. (2013), our system attempts to minimize any changes in behavior of the shark being

tracked by using a controller that circles and maintains a predetermined buffer distance from the shark instead of getting as close as possible.

3. SYSTEM OVERVIEW

3.1. OceanServer IVER2 AUV

The current system consists of two OceanServer Iver2 AUVs, although additional AUVs could be added. The Iver2 is a torpedo-shaped vehicle (see Figure 1(a)) with a rear propeller to provide locomotion, and four fins to control the vehicle's pitch, roll and yaw angles. The sensor payload used to determine the AUV state includes a pressure sensor for depth, a 3-DOF compass, a wireless antenna, a GPS receiver, and a six-beam Doppler velocity logger. It is equipped with two processors, a primary and secondary, each running an embedded Windows operating system. The primary processor communicates with the AUV's sensors and actuators. The secondary processor interfaces with the primary via an RS-232 serial port and hosts the user programmed control, estimation and communication systems. The AUVs broadcast their current position and sensor measurements to each other via a WHOI Micro-Modem (Freitag et al., 2005) and externally mounted transducers, allowing for cooperative tracking and following of the tagged marine animal.

In addition, each AUV is outfitted with a Lotek MAP RT receiver and an associated stereo-hydrophone set, designed to listen for acoustic signals at a frequency of 76 kHz. The hydrophones are fixed to the AUV using a PVC frame that positions the omnidirectional hydrophones approximately 0.40 m below the AUV and at opposite ends of the AUV, that is, just ahead of the nose and just behind the tail. As suggested by Lotek, the separation distance between the hydrophones is 2.4 m (see Figure 1(a)). These hydrophones receive transmissions from Lotek acoustic tags, which transmit at 76.8 kHz.

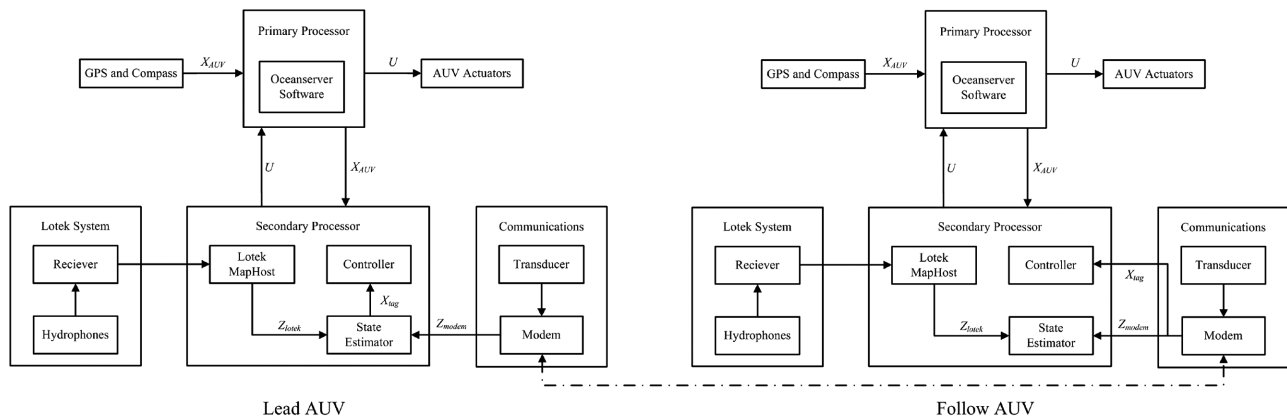The system uses a hierachical Leader/Follower control system to handle multi-vehicle coordination. The flow

Figure 2. Flow control within an AUV.

control within the *Lead* AUV is shown on the left side of Figure 2. The *Lotek System* hydrophones receive acoustic signals from fish tags, and the receiver board will send the time-of-arrival measurements from both hydrophones to the Lotek MapHost software running on the secondary processor. The MapHost software writes all measurements Z_{lotek} to a text file, making it accessible to the state estimator. These time measurements are first converted to bearing-to-tag and distance-to-tag measurements before being used by a particle filter to calculate fish state estimates.

In parallel, Lotek measurements and AUV states sent from the *Follower* AUVs are received through the acoustic modem *Communication* system. These measurements Z_{modem} are also used by the particle filter for state estimation. Details of the state estimation are provided in Section 4.

The estimated state of the tagged fish is passed to the AUV's *controller*, which uses a combination of a path planning algorithm for obstacle avoidance and a path following control law to drive the AUV toward the tagged fish. Once the AUV is within the local vicinity of the tagged fish, the controller invokes a decentralized target circumnavigational controller described in detail in Tang et al. (2012). The AUVs will circumnavigate on the current estimate of the tag position (see Figure 1(c)) and transition to circumnavigate a newer estimate of the tag position when it has moved past a threshold distance.

The controller sends the commands U of desired propeller rotation speed and fin angle to the Primary Processor via serial RS-232 communication. The OceanServer software package relays U to the AUV actuators, that is, the propeller motor and fin motors. To calculate U, the controller uses closed-loop control laws that require feedback in the form of planar position, depth, roll, pitch, and yaw states X_{AUV} as estimated by the OceanServer software. When the vehicle is on the surface, its planar position is estimated by fusing DVL, compass, and GPS. To understand errors

associated with the GPS receiver, stationary vehicle tests were performed in which GPS measurements were logged for several minutes to yield a standard deviation on the order of 4.5 m. When underwater, the AUV state is estimated by fusing only the depth sensor, DVL, and compass measurements. Details of the controller are found in Section 5.
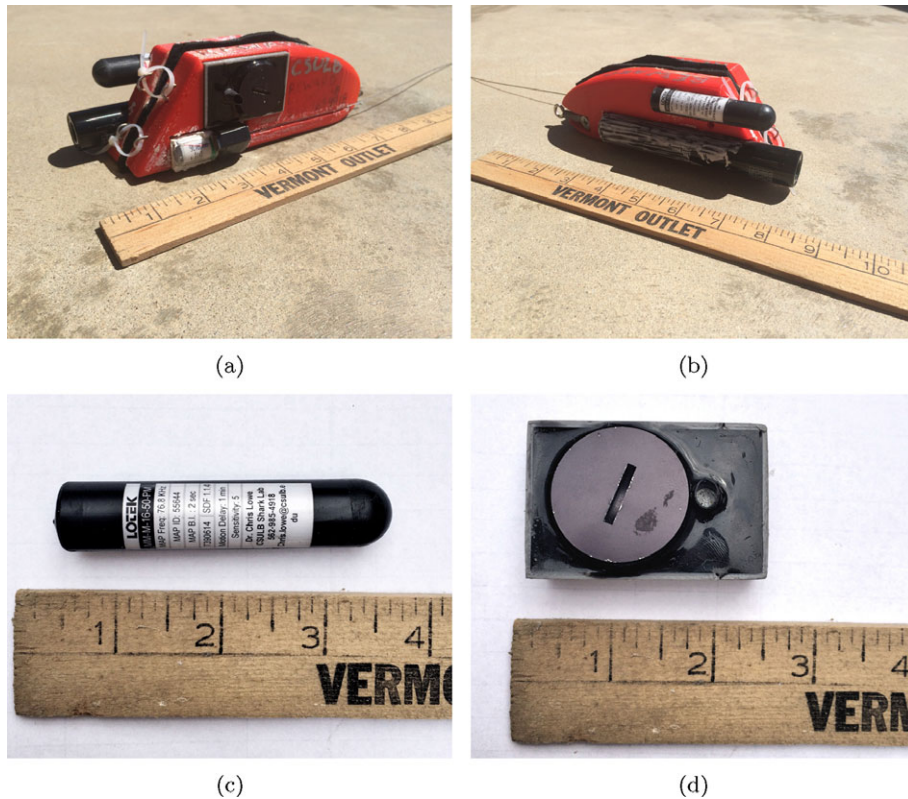
Flow control within the *Follower* AUV is almost identical. However, it does not rely on its own state estimates for controlling the AUV. Instead, it uses the *Lead* AUV's most recently calculated state estimate of the tag position X_{tag} as the target point to drive toward and circumnavigate. This tag position is sent from the *Lead* AUV using the acoustic modem. Each transmission takes 5 s to complete, and only one AUV can transmit at a time, leading to a communication period of 10 s. In this way, both AUVs will circumnavigate the same target point and avoid collision with one another.

3.2. SmartTag Package

The AUVs described above have been modified to track acoustic tags. In previous work by the authors, researchers attached an off-the-shelf acoustic tag to the dorsal fin of a shark with a dart. Recovering such tags is unnecessary because all information is telemetered. However, transmitting all data from from IMUs with high-sampling frequency is not feasible due to bandwidth limitations, signal attenuation, and power consumption. Hence, logging such measurements is required, and the tag logger must be retrieved after the experiment. To address this requirement, a tag package was developed that clamps onto the dorsal fin of the shark and utilizes a timed release mechanism (see Figures 1(b) and 3). We call this tag package a *SmartTag*.

The shell of the SmartTag is 3D printed and filled with micro-balloon epoxy foam for structural rigidity and buoyancy. It not only holds a Lotek acoustic tag but also carries

Figure 3. The SmartTag package: Two views (a) and (b). The green rectangle indicates the position of the IMU. The bottom dark cylinder is the video logger system. The top dark cylinder is the acoustic tag. The white cylinder is the VHF transmitter. The Lotek acoustic tag (c). The Loggerhead OpenTag IMU (d).

a Loggerhead OpenTag 9-DOF (gyroscope, accelerometer, magnetometer) IMU, a Little Leonardo video logger, and a VHF transmitter. The front of the tag is held together by zip ties and the rear by burn wires. The tag package is positively buoyant; it is designed so that the portion holding the Lotek tag floats in the water, and the antenna of the VHF transmitter floats above the water. This allows the tag to be located both acoustically and with a VHF receiver, providing two levels of redundancies for recovery. Described below are the two main components of the SmartTag.

3.2.1. Lotek Acoustic Tag System

Embedded in this SmartTag is the Lotek MM-M-16-50-PM acoustic tag preset to transmit a signal every 2 s (Figure 3(c)). The tag has a 30-day battery life and has an embedded pressure sensor whose measurements are encoded into the tag signal transmission. Depth is calculated by linearly extrapolating the pressure readings. The two hydrophones of the stereo-hydrophone system are mounted 2.4 m apart and suspended 0.4 m beneath each AUV. The separation of the hydrophones allows the angle between the AUV and

the acoustic tag to be calculated. This is done by assuming that the tag is sufficiently far enough (more than 5 m) from the two hydrophones such that the two line segments connecting the tag to the front and rear hydrophones are close to parallel, allowing for a trigonometric relation to be derived between distance from time of arrival and bearing to tag. The bearing measurement obtained with this method has a standard deviation of approximately $10°$. See Forney et al. (2012) for more details.

Because of the periodic nature of the tag transmissions, it is possible to extrapolate and predict the time of transmission from some initial transmission time t_0 and the transmission period T. Suppose that the tag transmits with a period T. Let z_{toa} be the time of detection, where $t_0 < z_{toa}$. The integer number of tag transmissions since t_0 is given by:

$$k = \text{Round} \left[\frac{z_{toa} - t_0}{T} \right]. \tag{1}$$

Thus, the estimated time of the transmission can be calculated by $t_{transmit} = t_0 + kT$. This allows the time of flight

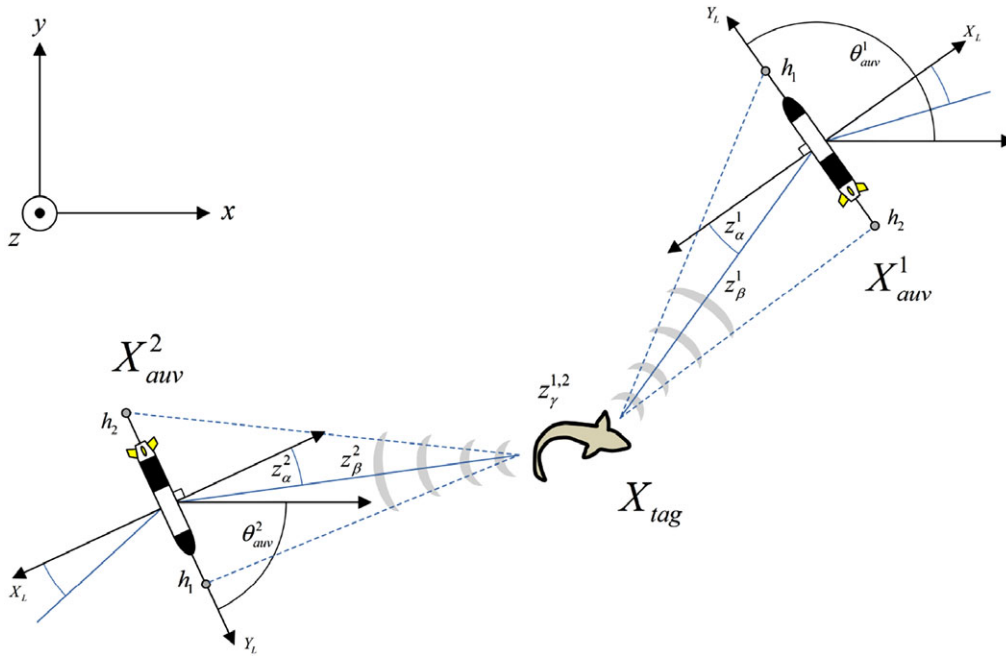**Figure 4.** An overview of the state estimation problem.

distance-to-tag to be calculated as $z_\beta = (z_{toa} - t_{transmit})c$, where c is the speed of sound in water. More details are presented in Lin et al. (2013) in which experiments show that, with proper calibration, the calculated distance has an error with a mean and a standard deviation on the order of 2 m over a time span of 4 h, with a drift of 1.5 m over a time span of 22 h.

3.2.2. Loggerhead OpenTag IMU

The Loggerhead OpenTag IMU (see Figure 3(d)) has a triaxial accelerometer, gyroscope, and magnetometer. It is capable of sampling at up to 100 Hz for a duration of 72 h. Data collected are stored on a micro-SD memory card. It also has an onboard pressure sensor capable of sampling at 10 Hz. The OpenTag IMU has a 3.7-V output pin that is connected to the burn wires holding the rear of the tag together. This output can be programmed to turn on only after a certain amount of time has passed and is the main timed release mechanism. As a fail-safe backup, a galvanic release is also used.

4. STATE ESTIMATION

4.1. State Estimation Problem

A two-dimensional (2D) overview of the state estimation problem is shown in Figure 4. The state of the ith AUV and sensor measurements at time t are denoted by $X_{auv,t}^i$ and Z_t^i,

respectively. The hydrophones h_1 and h_2 are mounted on the nose and tail ends of the AUV and the difference in time of arrival of a tag transmission is used to calculate the angle to the tag (with a sign ambiguity), denoted by z_α^i. Using the time of arrival measurement, the distance-to-tag z_β^i is calculated as described in Section 3.2.1. The depth of the tag z_γ^i is determined using the measurement transmitted from the tag. If the SmartTag is used, the 3-DOF magnetometer measurements $\vec{m}$, 3-DOF gyroscope measurements $\vec{g}$, and 3-DOF accelerometer measurements $\vec{a}$ from the IMU can also be used for state estimation.

The state estimation problem is defined as follows. Given a system of n AUVs at time t, where the ith AUV has the state

$$X_{auv,t}^i = [x_{auv}^i \ y_{auv}^i \ z_{auv}^i \ \theta_{auv}^i]_t \qquad (2)$$

and sensor measurements

$$Z_t^i = [z_\alpha^i \ z_\beta^i \ z_\gamma^i]_t \quad \text{and} \quad Z_t^{imu} = [\vec{m} \ \vec{g} \ \vec{a}]_t \qquad (3)$$

determine the tag state

$$X_{tag,t} = [x_{tag} \ y_{tag} \ z_{tag} \ \theta_{tag}]_t. \qquad (4)$$

The state estimator must also handle incomplete sensor measurements, such as the case of Z_t^i only containing a valid distance measurement z_β^i but invalid angle and depth measurements. In general, the acoustic measurements are not reliable due to occlusions and interference from

ambient noise in the underwater environment (e.g., kelp, reef structures).

4.2. Particle Filter Overview

The state estimator is based on a particle filter (Thrun, 2002; Thrun, Burgard, & Fox, 2005). To represent the belief state at time t, the particle filter uses a set of particles denoted by P_t. Each particle $p \in P_t$ is represented by the set $\{X_{tag}^p, w^p\}$ containing a tag state X_{tag}^p and weight w^p. The estimated tag state $X_{tag,t}$ at any time step t is the average of $X_{tag}^p \forall\, p \in P_t$. At initialization, P_t is filled with particles whose xyz coordinates are sampled randomly from uniform distributions. The algorithm for one time step of the state estimator is shown in Algorithm 1.

Algorithm 1 Multi-AUV State Estimator

1: $//Prediction$
2: **for** $p \in P_t$ **do**
3:     $X_{tag}^p \in p \leftarrow$ Motion_Model(X_{tag}^p, Z^{imu})
4:     **for** i from $1 : n$ **do**
5:         $\alpha_{exp}^p \leftarrow$ Expected_Angle$(X_{auv,t}^i, X_{tag}^p)$
6:         $\beta_{exp}^p \leftarrow$ Euclidean_Dist$(X_{auv,t}^i, X_{tag}^p)$
7:         $\gamma_{exp}^p \leftarrow z_{tag} \in X_{tag}^p$
8:         $w_p \leftarrow W(z_\gamma^i, \gamma_{exp}^p, \sigma_\gamma) * W(z_\beta^i, \beta_{exp}^p, \sigma_\beta) * W(z_\alpha^i, \alpha_{exp}^p, \sigma_\alpha)$
9:     **end for**
10: **end for**
11: $//Correction$
12: **if** there are valid measurements **then**
13:     **for** $1 : |P_t|$ **do**
14:         choose $p \in P_t$ with probability $\propto w_p$
15:         add p to P_{t+1}
16:     **end for**
17: **else**
18:     $P_{t+1} \leftarrow P_t$
19: **end if**

At each time step, the set of particles is propagated based on a motion model (Algorithm 1, Line 3). The particle weights w_p are calculated using the n AUV states and corresponding sensor measurements (Algorithm 1, Lines 5–8). The expected angle measurement (Algorithm 1, Line 5) can be calculated as:

$$\alpha_{exp}^p = \arccos\left(\frac{\vec{\theta} \cdot \vec{p}}{\|\vec{\theta}\| \|\vec{p}\|}\right) - \frac{\pi}{2}, \tag{5}$$

where

$$\vec{\theta} = [\cos(\theta_{auv}^i) \; \sin(\theta_{auv}^i) \; 0], \tag{6}$$

and

$$\vec{p} = [x_{auv}^i \; y_{auv}^i \; z_{auv}^i] - [x_{tag}^P \; y_{tag}^P \; z_{tag}^P]. \tag{7}$$

The weighting function W implements a Gaussian probability density function (Forney et al., 2012). If there are valid measurements, the particles are re-sampled based on their weights to create a new set of particles (Algorithm 1, Lines 13-16).

In Algorithm 1, the particle set is resampled (Lines 12–16) based on the value of particle weights as calculated in Line 8. For some measurement z_s, with expected measurement s_{exp}^p and standard deviation σ_s corresponding to particle p (where $s \in \{\alpha, \beta, \gamma\}$), the weight function $W(z_s, s_{exp}^p, \sigma_s)$ implements a Gaussian distribution function given by

$$W(z_s, s_{exp}^p, \sigma_s) = \frac{1}{\sqrt{2\pi}\sigma_s} e^{\frac{-(s_{exp}^p - z_s)^2}{2\sigma_s^2}}. \tag{8}$$

For z_α, z_β, and z_γ, the standard deviations used are determined experimentally and shown in Table I.

4.3. Motion Model

Two different Motion_Model() functions can be used to propagate the particles in the prediction step of (Algorithm 1, Line 3). One motion model is used when the AUV is estimating the location of the shark in real time. This is referred to as the stochastic motion model. During postprocessing offline, a second motion model that incorporates measurements from the OpenTag IMU can be used to refine the shark state estimates. The two different motion models are described in Sections 4.3.1 and 4.3.2.

4.3.1. Online Motion Model

For online state estimation, when the AUV is actively following a tagged fish, a stochastic motion model is used in the prediction step of the particle filter to propagate particles. The hybrid Brownian and Levy Flight motion model

Table I. Motion model and weight function parameters used in Algorithm 1 and Algorithm 2.

Parameter	σ_v (ms^{-1})	σ_{vz} (ms^{-1})	k (ms^{-1})	λ (ms^{-1})	ρ	ϕ	σ_α (red)	σ_γ (m)	σ_β (m)
Value	1	0.8	0.5	1	0.66	0.05	$\pi/18$	0.75	2

used is described in detail in Lin et al. (2014) and presented here in Algorithm 2.

Algorithm 2 Hybrid Random Walk Motion Model

1:     $\theta_{tag}^p \leftarrow$ UniformDistribution$(0, 2\pi)$
2:     $v_{tag}^z \leftarrow$ NormalDistribution$(0, \sigma_{vz})$
3:     // ρ is a number between 0 and 1
4:     **if** $\rho \geq$ UniformDistribution$(0, 1)$ **then**
5:         $v_{tag}^{xy} \leftarrow$ ParetoDistribution(k, λ)
6:     **else**
7:         $v_{tag}^{xy} \leftarrow$ Abs(NormalDistribution$(0, \sigma_v)$)
8:     **end if**
9:     $x_{tag}^p \leftarrow x_{tag}^p + |v_{tag}^{xy}| \cos(\theta_{tag}^p)\Delta t$
10:    $y_{tag}^p \leftarrow y_{tag}^p + |v_{tag}^{xy}| \sin(\theta_{tag}^p)\Delta t$
11:    $z_{tag}^p \leftarrow z_{tag}^p + v_{tag}^z \Delta t$

The hybrid motion model is designed to represent the "loitering" and "darting" motion behaviors of the tagged fish. At each time step, the motion model chooses with probability ρ and $1 - \rho$ of being in the loitering and darting state (Algorithm 2, Lines 4–8). To represent the loitering behavior of the tagged fish, a Brownian random walk motion model, which draws its speed at a single time step from a normal distribution centered at 0, is used. To represent the darting state of the tagged fish, a Levy Flight motion model, which draws its speed from a tail-heavy distribution (Pareto distribution with scale and shape parameter of k and λ, respectively) is used. Table I provides the parameter values used for this model.

4.3.2. Offline Motion Model

After the AUV tracking experiments are complete, the SmartTag package can be recovered. The IMU measurements from the SmartTag can be used within a more accurate motion model for offline state estimation. Specifically, the measurements from the OpenTag IMU are used to calculate an estimated heading and speed that can be used for particle propagation in the Motion Model of the prediction step. To note, the IMU logger must be time synchronized with

the AUVs measurement logging and is done by recording the UTC time that the IMU logger is turned on.

Magnetometer data from the IMU can be used to estimate the heading of the tagged individual. Because the tag is attached rigidly to the dorsal fin, the heading of the tag is used as an estimate of the heading of the shark. As the OpenTag is attached perpendicular to the xy horizontal plane, only the y and z axis of the magnetometer are used (see Figure 5(b)).

Before the magnetometer readings can be used, the magnetometer reading must be first corrected for hard and soft iron distortion. To accomplish this correction, let $\vec{m}_{max} = [m_{max}^y \; m_{max}^z]$ and $\vec{m}_{min} = [m_{max}^y \; m_{max}^z]$ be two vectors containing the maximum and minimum yz magnetometer readings, respectively. An offset $\vec{m}_{offset} = [m_{offset}^y \; m_{offset}^z]$ is calculated using Eq. (9).

$$\vec{m}_{offset} = \frac{\vec{m}_{max} + \vec{m}_{min}}{2} \tag{9}$$

The uncorrected yz magnetometer readings $\vec{m}_u = [m_u^y \; m_u^z]$ are corrected for hard iron distortion by subtracting by $\vec{m}_{offset}$.

$$\vec{m}_{hc} = \vec{m}_u - \vec{m}_{offset} \tag{10}$$

To correct for soft iron calibration, an ellipse centered at $(0, 0)$ with semi-diameters a and b, with the a axis rotated by ϕ relative to the y axis, is fitted using least squares to the readings corrected for hard iron distortion. In polar form, the equation describing such an ellipse is given by

$$r(\theta) = \frac{ab\sqrt{2}}{\sqrt{(b^2 - a^2)\cos(2\theta - 2\phi) + a^2 + b^2}}. \tag{11}$$

After fitting for a, b, and ϕ in Eq. (11), a corrected yz magnetometer reading $\vec{m}_c = [m_c^y \; m_c^z]$ is calculated from the hard iron–corrected reading $\vec{m}_{hc}$ by Eq. (12). Here, $R(\phi)$ represents a rotational matrix and $\star$ denotes element-wise multiplication operation.

$$\vec{m}_c = R(\phi)((R(-\phi)\vec{m}_{hc}) \star [1, \; a/b]) \tag{12}$$

As the x axis of the OpenTag IMU is assumed parallel to the yaw axis of the shark body, gyroscope readings

(a)	(b)

Figure 5. An image of the tag on a leopard shark fin (a). The coordinate axis used for the magnetometer readings (b).

from the x axis are used as a measure of tail beat. A continuous wavelet transform of x axis gyroscope data provides tail beat frequency as a function of time, which can then be used to determine swim speed. For the leopard shark, experiments done in (Scharold, Lai, Lowell, & Graham, 1989) demonstrated a linear relationship between tail beat frequency and swim speed given by:

$$f = 9.42 + 82.65v, \tag{13}$$

where f is the tail beat frequency in hertz and v is the swim speed in body lengths per second. Eq. (13) can be manipulated to determine a shark's swim speed from the calculated tail beat frequency and measured body length.

Given an estimate of heading and speed of the shark at each time step, the motion model used for propagation by the offline state estimator is described by Algorithm 3. Instead of drawing the speed and heading from a random distribution, the speed and heading of each particle is set by adding random noise to the estimated speed and heading of the shark (Algorithm 3, Lines 1–2).

Algorithm 3 Propagation with Heading and Speed

1:     $\theta_{tag}^p \leftarrow \theta_{est} + \text{NormalDistribution}(0, \sigma_\theta)$
2:     $v_{tag}^{xy} \leftarrow v_{est}^{xy} + \text{NormalDistribution}(0, \sigma_v)$
3:     $v_{tag}^z \leftarrow \text{NormalDistribution}(0, \sigma_{vz})$
4:     $x_{tag}^p \leftarrow x_{tag}^p + |v_{tag}^{xy}| \cos(\theta_{tag}^p) \Delta t$
5:     $y_{tag}^p \leftarrow y_{tag}^p + |v_{tag}^{xy}| \sin(\theta_{tag}^p) \Delta t$
6:     $z_{tag}^p \leftarrow z_{tag}^p + v_{tag}^z \Delta t$

---

5. MULTI-AUV CONTROL SYSTEM

Given an estimated fish tag position, as calculated by the particle filter described above, the multi-AUV control system will drive the AUVs to follow the tagged fish. At the high level, the control system consists of three subsystems. The first subsystem, the motion planner, invokes an A* path planner to construct a collision-free path T to the goal location X_{des}. This goal location is calculated as the position closest to the estimated tag position X_{tag} that lies within a preset boundary map.

The second subsystem, the position tracking controller, is used by the AUVs to fly toward X_{des} by following the path T constructed by the motion planner. Once an AUV is within a distance d of X_{des}, the third subsystem, called the circle tracking controller, is used to by the AUV to circumnavigate X_{des}. This enables the AUVs to obtain multiple sensor vantage points without being so close as to alter fish behavior. Algorithm 4 provides details of how switching between the two control subsystems occurs. In this algorithm,

the control signal vector is U, which contains the desired propeller speed and fin angles sent to the actuators.

Algorithm 4 Control Subsystem Selection

1:     $(T, X_{des}) \leftarrow \text{MotionPlanner}(X_{AUV}, X_{tag})$
2:     $dist \leftarrow \sqrt{(x_{auv} - x_{des})^2 + (y_{auv} - y_{des})^2}$
3:
4:     **if** $dist > D$ **then**
5:        $U \leftarrow \text{PositionTrackingControl}(X_{AUV}, T)$
6:     **else**
7:        $U \leftarrow \text{CircleTrackingControl}(X_{AUV}, X_{des})$
8:
9:     **end if**
10:    **return** U

5.1. Motion Planner

The motion planner is used to both determine a desired position to track, as well as construct a collision-free path to the desired position. The path should be minimal in length and include desired depths that enable in situ collection of environment measurements (e.g., temperature). This allows the AUV to not just track the tagged fish but also characterize the fish's habitat.

The desired goal position of the AUV $X_{des} = [x_{des} \ y_{des}]$ is selected based on the current estimated position of the fish and the free navigable space of the environment, as dictated by a previously constructed 2D occupancy grid map M. In general, the desired goal position is calculated as the point in the free space of M closest to the AUV that is lying on a circle of radius d centered on the current fish position estimate (see Figure 6(a)). If no such point lying within the free space of M exists, then the desired goal position is calculated to be the point closest to the fish position estimate within the free space of M that lies on the line segment connecting X_{tag} to X_{AUV} (see Figure 6(b)).

Once a desired goal point X_{des} has been determined, a collision-free path to X_{des} must be constructed. The field of motion planning has generated a large number of algorithms capable of constructing collision-free robot paths in low-dimensional and high-dimensional spaces (Latombe, 1991; LaValle, 2006). In this case, M is a 2D discretized grid map of relatively low dimensionality (e.g., 50 × 50). Hence, an exhaustive search like the standard A* algorithm Hart, Nilsson, & Raphael (1968) can be employed on M to find the optimal 2D planar collision-free path to X_{des}. The x, y coordinates of this path are augmented with desired depths (e.g., 1 m below surface) to create a 2D collision-free path T for underwater environment data collection. To prevent repeated unnecessary replanning due to noise in the estimated position of the fish, X_{des}, is updated and a new A* search is done only when the estimated
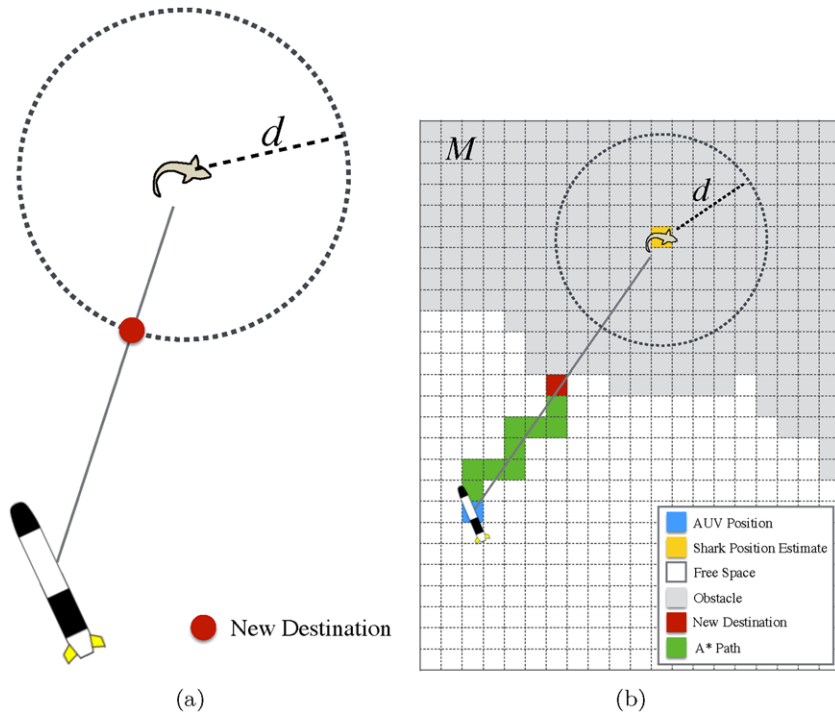
Figure 6. Finding new destinations: Clear from obstacle (a), Blocked by obstacles (b).

position of the fish has moved by a distance of d from the previous X_{des}.

5.2. Position Tracking Controller

The position tracking controller is used when the estimated position of the shark is greater than some threshold distance d from the AUV's position. It directs the AUV to follow the path T using the low-level closed-loop controller described below in Figure 7.

The position tracking controller combines a yaw (ψ) controller and hybrid pitch (θ) and roll (ϕ) controller as shown in Figure 7. The yaw controller utilizes a standard proportional control law to adjust the rudder fin angle based on the heading error. In Eq. (14), ψ_d and ψ are the desired and measured yaw angles, respectively. The angle ψ_d is set to be in the direction of the next point to track on the trajectory T. K_ψ is the proportional control gain. The desired rudder fin angle, δ_{rudder}, is the control signal sent to the AUV's rudder fins servo motors.

$$\delta_{rudder} = K_\psi(\psi_d - \psi). \quad (14)$$

The hybrid depth and roll controller is a cascaded proportional-integral-derivative (PID) controller system.

The first PID controller accepts a desired depth value, z_d, and converts it to a desired pitch angle, θ_d.

$$\theta_d = K_{P,z}(z_d - z) + K_{I,z} \int (z_d - z)dt + K_{D,z}\frac{d}{dt}(z_d - z). \quad (15)$$

The second PID controller accepts the desired pitch angle, θ_d, and outputs a desired fin angle, δ_{pitch}. In addition to the depth controller, a roll controller is added to further adjust the fin angle to control the roll of the robot during a dive using a proportional controller. The output of the roll controller is denoted as δ_{roll}. The assignments of port and starboard fin angles can be described in Eqs. (16), (17), and (18).

$$\delta_{pitch} = K_{P,\theta}(\theta_d - \theta) + K_{I,\theta} \int (\theta_d - \theta)dt + K_{D,\theta}\frac{d}{dt}(\theta_d - \theta) \quad (16)$$

$$\delta_{roll} = K_\phi(\phi_d - \phi) \quad (17)$$

$$\delta_{port} = \delta_{starboard} = \delta_{pitch} + \delta_{roll}. \quad (18)$$

The port and starboard fin angles are then set as the sum of the pitch and roll control pitch fin control angles. The gains for the depth, pitch, and roll controller, $K_{P,z}$, $K_{I,z}$, $K_{D,z}$, $K_{P,\theta}$, $K_{I,\theta}$, $K_{D,\theta}$, K_ϕ, were experimentally determined after the AUV was properly ballasted in seawater.
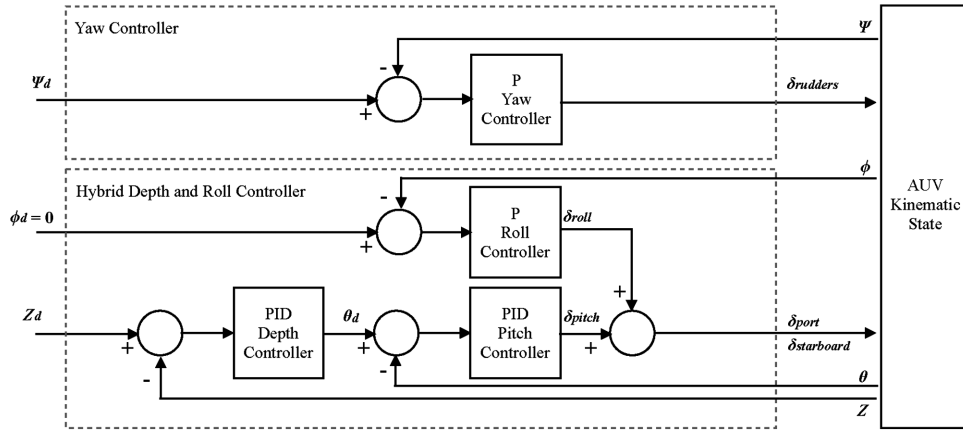
Figure 7. Position tracking controller diagram.

5.3. Circle Tracking Controller

Once the AUV is within the threshold distance d of the estimated shark position, the autonomous control system invokes a circle tracking controller. In this state, the AUV uses a modified version of the target circumnavigational controller previously developed by the authors (Tang et al., 2012). The goal of this controller is to drive the AUVs in a circle of radius R_{des} and space the AUVs apart on this circle with phase difference $\Delta\gamma_{des}$ (see Figure 8). This can be achieved by minimizing the following control errors for the ith AUV:

$$\rho_{i,t} = R_{des} - \sqrt{(x^i_{auv} - x^i_{des})^2 + (y^i_{auv} - y^i_{des})^2} \quad (19)$$

$$\beta_{i,t} = \left[\text{atan2}(y^i_{auv} - y^i_{des}, x^i_{auv} - x^i_{des}) - \frac{\pi}{2}\right] - \psi_{i,t} \quad (20)$$

$$e_{i,t} = \Delta\gamma_{des} - [\gamma_{i+1,t} - \gamma_{i,t}]. \quad (21)$$

In the first of the above error equations, $\rho_{i,t}$ is the difference between the circle radius R_{des} and the distance to the goal target located at $[x_{des}\, y_{des}]$ at time step t. The second error equation defines $\beta_{i,t}$ as the difference between the desired yaw angle, that is, the angle of the line tangent to the circle for the AUV's current phase γ, and the current yaw angle $\psi_{i,t}$. The last error equation defines $e_{i,t}$ as the difference between the desired phase difference between AUVs and the current estimated phase difference of two AUVs in the multi-AUV system, specifically AUV$_i$ and AUV$_{i+1}$, which follows directly behind AUV$_i$ on the circle.

To minimize these errors, the following control variables $\omega_{i,t}$ and $v_{i,t}$ for the ith AUV can be set with the following proposed control laws. In this case, the desired AUV angular velocity $\omega_{i,t}$ and linear velocity $v_{i,t}$ are assumed to be trackable (as verified in Tang et al., 2012).

$$\omega_{i,t} = -\frac{v_{i,t}\cos(\beta_{i,t})}{R_{des} - \rho_{i,t}} + \frac{K_\beta}{\Delta t}\beta_{i,t} + \frac{K_\rho}{\Delta t}\rho_{i,t} \quad (22)$$
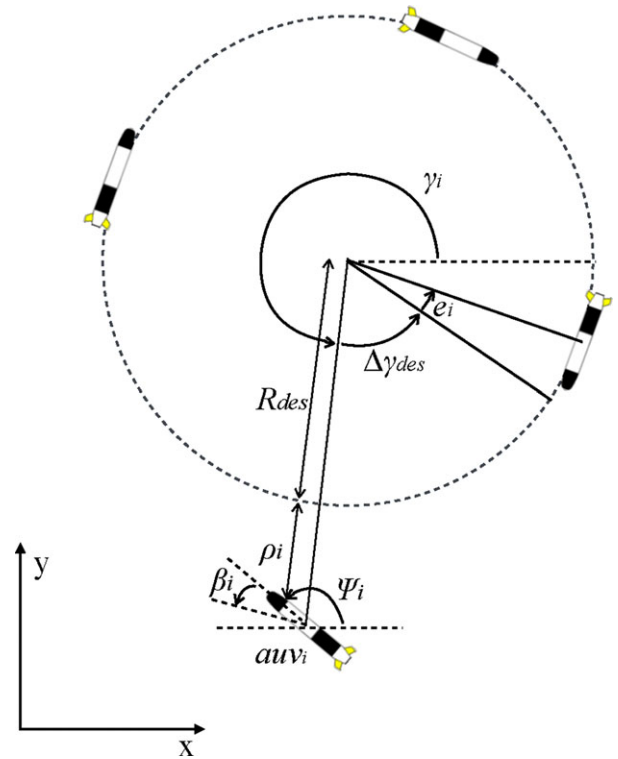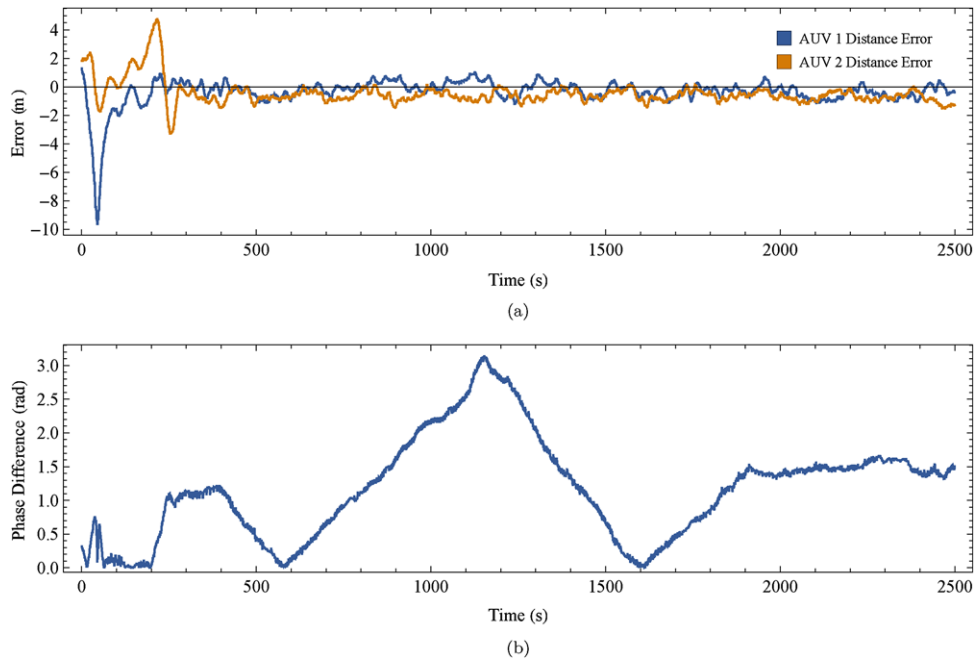

Figure 8. The desired radius from the target is R_{des}. The angle error between desired heading to the current heading is β. The distance error between R_{des} and the current radius from the target is ρ, and the error between the desired phase, $\Delta\gamma$, to the current phase is e.

$$v_{i,t} = -\frac{R_{des} - \rho_{i,t}}{R_{des}\cos(\beta_{i,t})}\left(V_{nom} + \frac{R_{des}K_\gamma}{\Delta t}(e_{i+1,t} - e_{i,t})\right) \quad (23)$$

In the above control laws, K_β, K_ρ, and K_γ are the proportional control gains. According to Tang et al. (2012), K_β and K_ρ must satisfy the following conditions for proven

Figure 9. Two AUV circling controller errors. Figure 9(a) shows the distance error, and Figure 9(b) shows the phase difference.

stability, which are dependent on the control loop time step Δt:

$$K_\rho > 0 \qquad (24)$$

$$0 \leq K_\beta \leq 4 \qquad (25)$$

$$\frac{2(K_\beta - 2)}{K_\rho \Delta t} \leq v_{i,t} \leq \frac{K_\beta^2}{4 K_\rho \Delta t}. \qquad (26)$$

The range of K_γ is dependent on the number of AUVs in the system. For example, for 3 AUVs, $0 < K_\gamma < 2/3$. More details about K_γ can be found in Tang et al. (2012).

6. VALIDATION EXPERIMENTS

A series of verification experiments were performed at Big Fisherman's Cove, Catalina Island, California. The cove is adjacent to the USC Wrigley Institute of Environmental Studies. Results validating the multi-AUV (Autonomous Underwater Vehicle) circle tracking controller are first presented below. To validate the performance of the multi-AUV state estimation, *boat-tracking* experiments and *shark-tracking* experiments were conducted.

For boat-tracking experiments, an acoustic tag was hung from a moving boat with a 2-m line. The boat was driven around the cove at various speeds up to $2.0\,ms^{-1}$, and the true state of the boat was recorded every 2 s by a GPS receiver fixed to the boat. The GPS receiver used the Wide Area Augmentation System (WAAS) to provide an ac-

curacy of 1 to 3 m. Examples of the trajectories taken by the boat can be seen in Figure 10. Although the boat followed such trajectories, AUV(s) were deployed to simultaneously estimate the boat state (i.e., 3D position and yaw orientation) and autonomously follow the boat. During shark-tracking experiments, a leopard shark was tagged and the AUVs were deployed to simultaneously estimate the shark state and autonomously follow the shark.

6.1. Control System Experiments

To demonstrate the effectiveness of the multi-AUV circum-navigation system, results of the two AUVs circling a fixed point are shown in Figure 9. The difference between the desired distance and actual distance (distance error) to the fixed points for both AUVs is shown in Figure 9(a). It can be seen that the distance error decreases quickly to an order of 1.0 to 2.0 m. The phase between the two AUVs is shown in Figure 9(b). The desired phase difference between the two AUVs is set to $\pi/2$. A significant amount of noise is expected given that waves and wind were present during all experiments.

6.2. Boat-Tracking Trials

Two sets of boat-tracking trials were conducted, one set using just the standard Lotek Tag and one set using the SmartTag that included both the Lotek Tag and an IMU.

Table II. State estimation position errors of January 2014 and July 2014 boat trials.

	January 2014 Boat Trials				July 2014 Boat Trials				
	Trial 1	Trial 2	Trial 3	Trial 4	Trial 1	Trial 2	Trial 3	Trial 4	Trial 5
Mean Err. (m)	8.0	6.8	13.7	8.8	5.4	8.6	10.4	9.6	7.6
Median Err. (m)	5.0	5.3	8.4	6.5	5.1	7.9	9.7	9.2	6.9
SD Err. (m)	10.5	4.8	13.2	8.4	2.5	5.2	5.4	5.9	4.6

6.2.1. January 2014 Trials

The first set of experiments were conducted during the month of January 2014. Two AUVs were deployed and commanded to circle a fixed point in the cove. The acoustic measurements obtained during this set of experiments were postprocessed offline using Algorithms 1 and 2 to estimate the boat's position as a function of time.
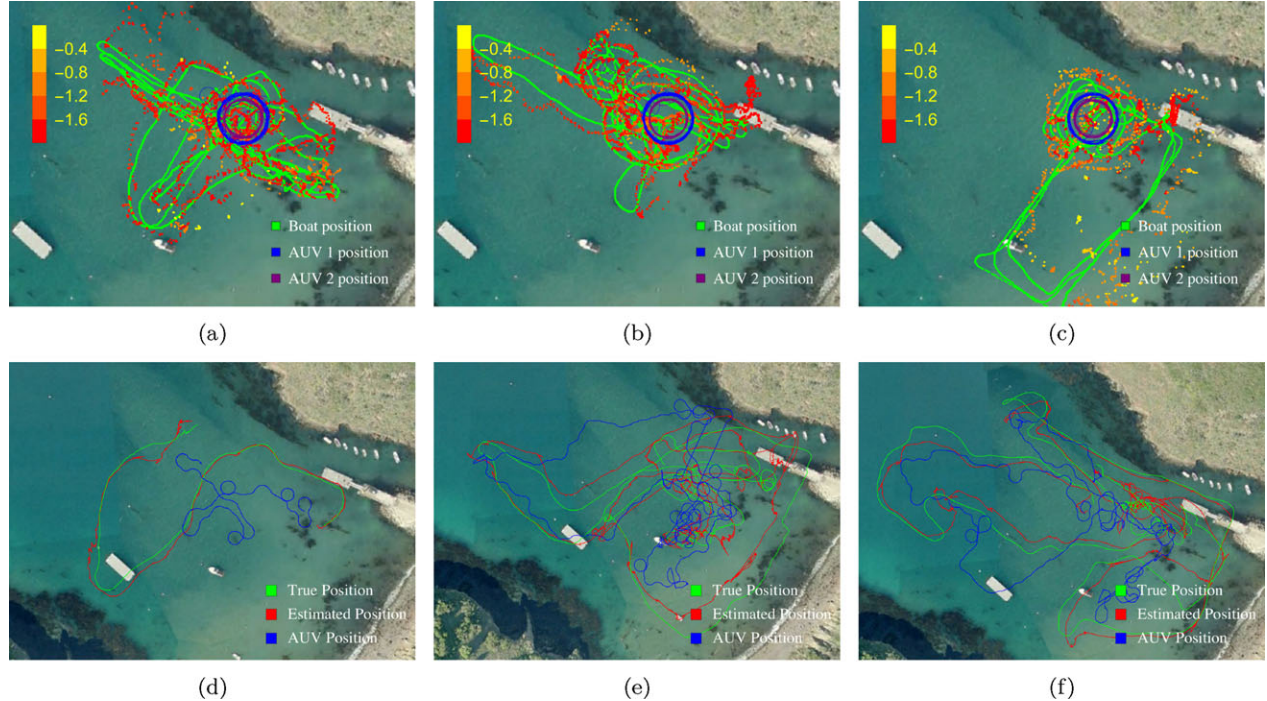
This set of boat-tracking experiments consisted of four separate trials, whose length varied from 20 to 45 min. The results of Trials 1, 2, and 3 are presented in Figure 10(a), 10(b), and 10(c), respectively. Note that these are the same results previously presented in Lin et al. (2014) and are presented here for the sake of completeness. The error in position is shown in Table II, where the position error at time t is defined by:

$$\epsilon_t^{pos} = \|\vec{x}_t^{est} - \vec{x}_t^{gps}\|. \tag{27}$$

In Eq. (27), $\vec{x}_t^{est}$ is the estimated xy position of the tag and $\vec{x}_t^{gps}$ is the true xy position of the tag as determined from linear interpolating over time the recorded boat GPS positions.

6.2.2. July 2014 Trials

The second set of boat-tracking experiments, that is, those that incorporated IMU data for state estimation, was conducted in July 2014. A single AUV used Algorithms 1 and 2 to estimate the position of the boat in real time. This allowed the AUV to actively follow the target using the position tracking controller described in Section 5.2. The measurements obtained from the AUV were then postprocessed offline with measurements from a Loggerhead IMU fixed to the boat, using the same state estimator but with a modified version of the motion model described in Algorithm 3.

(a)   (b)   (c)

(d)   (e)   (f)

Figure 10. Results of *Boat-Tracking Trials without IMU* (a), (b), and (c); the estimated tag locations are shown by the dots ranging from yellow to red, which corresponds to estimated tag depth (m) shown in the bar legend. Results of *Boat-Tracking Trials with IMU* (d), (e), and (f).

Table III. Average time between replanning for the July 2014 boat trials.

	Trial 1	Trial 2	Trial 3	Trial 4	Trial 5
Mean Time between Replans (s)	16.2	19.6	14.4	14.6	14.2

Specifically, because no tail beat frequency was available to estimate speed, the tag speed v_{tag}^{xy} (Algorithm 3, Line 2) was drawn from a normal distribution instead.

This second set of boat tracking experiments consisted of five trials. The length of the trials varied from 10 to 36 min. The results of Trials 1, 4, and 5 are shown in Figure 10(d), 10(e), and 10(f), respectively. The errors in position as calculated by Eq. (27) are shown in Table II. The average time between replanning (which happens when the tracking origin of the AUV has changed) is shown in Table III.

6.3. July 2013 Shark-Tracking Trials

On July 15, 2013, a single leopard shark was tagged and tracked during the mornings and afternoons of July 15 to 18. Algorithm 1 was used in combination with a Brownian motion model to estimate the position of the individual in real time and actively follow it. The measurements obtained were then postprocessed offline with the same state estimator but with the motion model described in Algorithm 3. The results of these shark trials are shown in Figure 11(c), which aggregates the data from six individual tracks. In total, 12.5 h of tracking data were collected. These trials used only the Lotek acoustic tag system that did not include an IMU. Within these tracks, the amount of time in which the AUVs were circling the estimated shark position versus the amount of time in which the AUVs were circling a point on the boundary is roughly equal.
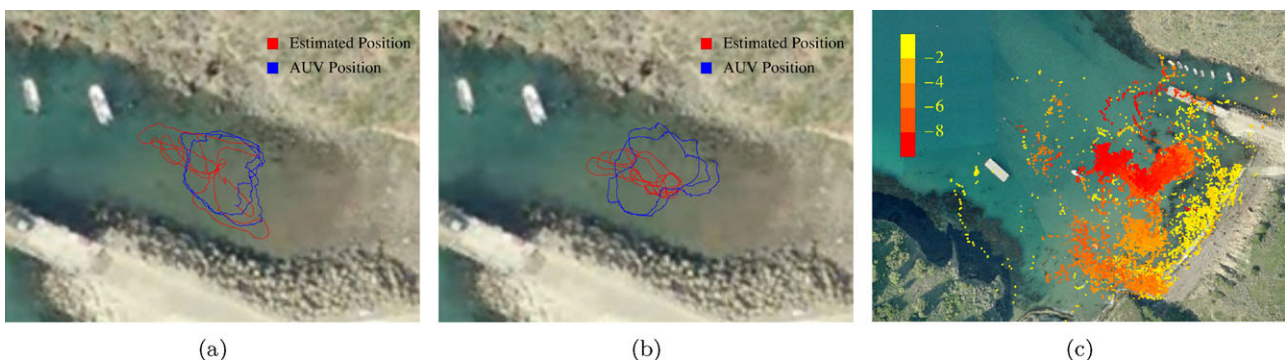
It was observed that shark locations were not distributed uniformly across the cove; instead, locations were aggregated. With the addition of the 3D location data, it is observed that the shark's depth is associated with the sea floor, as evidenced by deeper depths in deeper areas of the cove. Both of these observations agree with the known behavior of leopard sharks (Hight & Lowe, 2007).
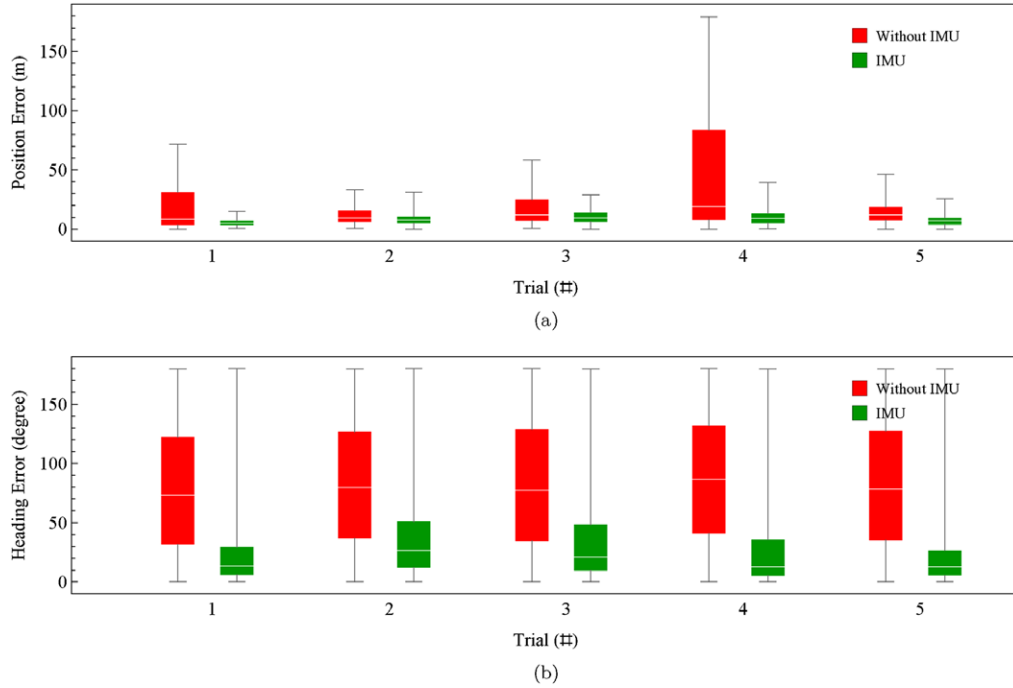
6.4. July 2014 Shark-Tracking Trials

Three different leopard sharks were tagged on different days in July 2014 using the tag package that included the Loggerhead IMU. Unlike previous shark-tracking trials, all three individuals stayed within a small area of the cove shown in Figure 11(a) and 11(b). Hence, only a single AUV was deployed to circle a fixed point in this area. The measurements obtained from the AUV were then postprocessed offline with measurements from the Loggerhead IMU fixed to the shark using Algorithms 1 and 3.

The results of a 50-min shark track conducted in July 24, 2014, are shown in Figure 11(a) and 11(b). In addition, two other tracks of two different individuals were conducted with the IMU, on July 18, 2014, and July 7, 2014, respectively, for a combined duration of 4.3 h. Compared to the previous summer, the tagged individual stayed within a small cove during duration of the track. Because of the limited maneuvering space for the AUV within the small cove, the AUV was set to circle a fixed point as opposed to actively following the tagged individual.

The results of the July 2014 tracks demonstrate one of the main advantages of the AUV tracking system over traditional methods such as active tracking with a boat. The cove in which the sharks stayed in were too small for boats to maneuver in. Therefore, active tracking with a boat would not be able to measure any movement of the shark other than detecting that it is in the cove. With the addition of IMU data, the measurements from the AUV tracking

(a)　　　　　　　　　　(b)　　　　　　　　　　(c)

Figure 11. Results of shark-tracking trials. Partial result of the July 24, 2014, tracks done with the SmartTag that incorporates IMU data (a) and (b). The shark location of the July 2013 tracks (c); the colors correspond to estimated depth of the tagged individual in meters.

Figure 12. Comparison of errors due with and without incorporation of IMU data, using data from trials in section 6.2.2. Position and heading errors are shown in Figure 12(a) and Figure 12(b) respectively.

system enabled observations of fine scale motion that were previously unattainable.

7. DISCUSSION OF RESULTS

7.1. Effect of IMU Measurement on State Estimation Accuracy

The incorporation of IMU data results in tracks with higher accuracy and precision, and can be quantified by analyzing the effect of IMU data on position error and heading error. This was accomplished by postprocessing the measurements from Section 6.2.2 with two different state estimators, one that incorporates the IMU data and one that does not. The difference in state estimation errors are then compared.

7.1.1. Comparison of Position Error

The effect of IMU data on position error is presented in Figure 12(a). The incorporation of IMU data leads to significantly lower position errors, for example, mean position errors decreased by 25% to 75%. Of particular significance is the decrease in the third quartile, maximum, and interquartile range of position errors, implying that the incorporation of IMU data produces tracks with less variation in error. It can also be seen from Table II that even though the *Boat-Tracking Trials with IMU* used only measurements from one
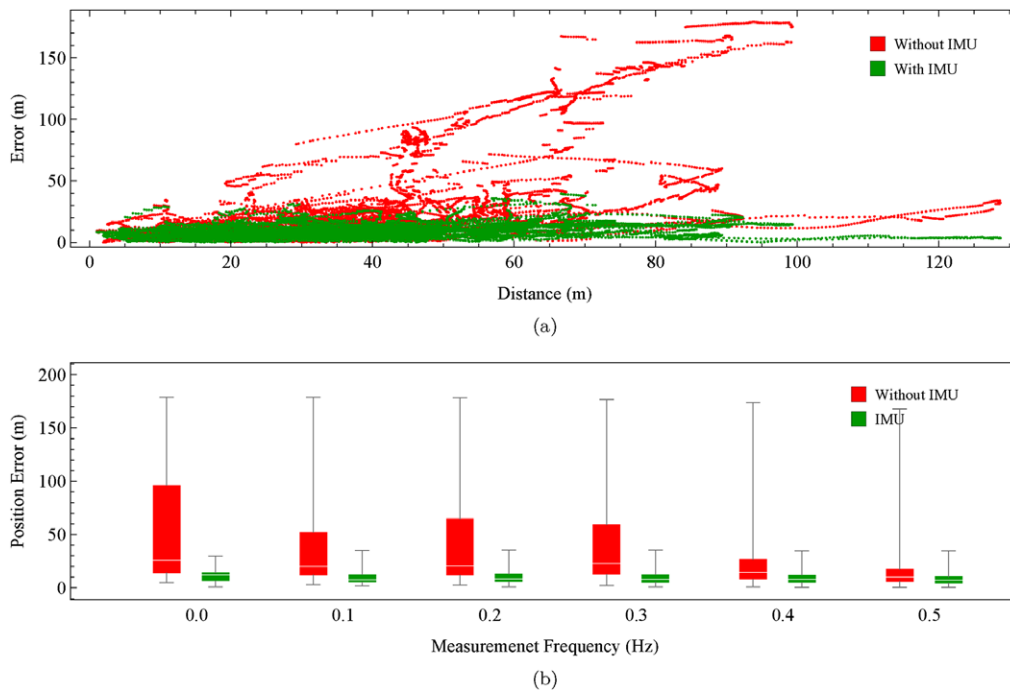
AUV, it was able to achieve a position error similar to that of *Boat-Tracking Trials without IMU*, which used measurements from two AUVs.

7.1.2. Comparison of Heading Error

The effect of IMU data on heading error is presented in Figure 12(b). Here, heading error at time t is given by

$$\epsilon_t^\theta = \arccos\left(\frac{\vec{\theta}_t^{est} \cdot \vec{\theta}_t^{gps}}{\|\vec{\theta}_t^{est}\|\|\vec{\theta}_t^{gps}\|}\right), \quad (28)$$

where $\vec{\theta}_t^{est}$ is the estimated xy heading vector of the tag and $\vec{\theta}_t^{gps} = \vec{x}_t^{gps} - \vec{x}_{t-1}^{gps}$ is the true heading of the tag. Without IMU data, the mean and median heading errors were on the order of $80°$ with an interquartile range on the order of $90°$. This is marginally better than estimating the heading by drawing from a random uniform distribution from $0°$ to $360°$, which would have resulted in a mean heading error of $90°$ if the true heading was uniformly distributed in the same range. By incorporating IMU data, the mean and median heading errors were on the order of $30°$ with an interquartile range on the order of $25°$. The decrease in heading error allows for the shape of the estimated track to resemble that of the true path even when position estimates are not accurate. This is illustrated visually in Figure 10.

Figure 13. Comparison of position error as a function of distance and frequency of sensor measurements due with and without incorporation of IMU data are presented in Figure 13(a) and Figure 13(b) respectively.

7.1.3. Position Error as a Function of Distance

An important metric of state estimation is the effect of distance to tag on the position error. Ideally, the AUVs will stay relatively close to the tagged target, but the physical constraint of the environment (i.e., shallow areas and kelp forests) could prevent the AUVs from being at the desired distance to target. Therefore, it is important the position error does not increase significantly as a function of distance to tag. The effect of distance to tag on position error is shown in Figure 13(a). It can be seen that without IMU measurements distance has a significant impact on position error. A linear fit of error as a function of distance gives a slope coefficient of 0.01 and 0.52 for data points with and without IMU measurements, respectively. Hence, using the IMU data reduces the sensitivity of position error to distance by an order of 50.

7.1.4. Position Error as a Function of Measurement Frequency
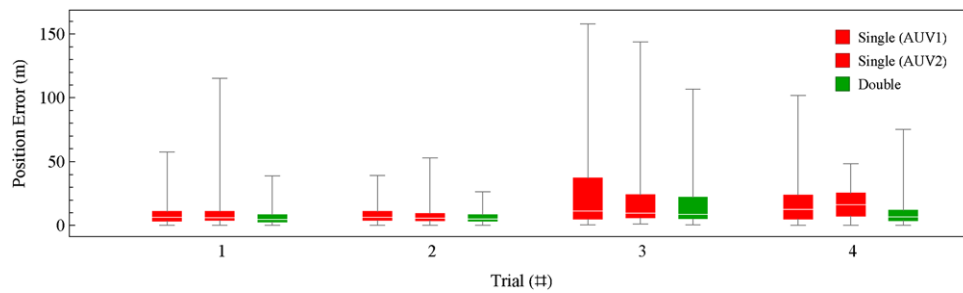
Another metric for the state estimation is the effect of the frequency of measurements detected by the hydrophones on position error. Ideally, the AUVs will be able to receive measurements at the tag transmission rate of 0.5 Hz. However, variation in the acoustic environment often cause decreases in the frequency of the measurements received.

Therefore, it is important that position error does not increase significantly as the frequency of measurements decrease. The effect of measurement frequency on position error is shown in Figure 13(b), in which the measurement frequency was estimated by using a moving average window of 20 data points. It can be seen that, without IMU measurements, a decrease in received measurement frequency has a more significant impact on position error compared to that with IMU measurements. A linear fit of error as a function of measurement frequency gives a slope coefficient of -3.64 and -73.75 for data points with and without IMU measurements, respectively. Hence, using the IMU data reduces the sensitivity of position error to acoustic signal reception rate by an order of 25.

7.2. Comparison of Tracking Accuracy of One versus Two AUVs

In a tracking situation with multiple AUVs, the additional vantage points to the tagged target can improve tracking accuracy. This was quantified by postprocessing the measurements from Section 6.2.1 with only measurements from one AUV and comparing the result with the same tracks that used measurements from both AUVs. The results are presented in Figure 14. The use of measurements from both AUVs leads to a reduction in mean and median errors by a factor of 2. Furthermore, Figure 14 shows that there is a

Figure 14. Comparison of position error distribution of boat trials using one versus two AUV(s). The two box whisker plots for single AUV tracks in each trial corresponds to the distribution of errors using measurements from each AUV.

similar reduction in the interquartile range when both AUVs are used.

8. CONCLUSION

The multi-AUV system presented in this paper has demonstrated the ability for a mobile underwater robot sensor system to autonomously track and follow tagged fish with meter-level positioning accuracy. When using the newly developed SmartTag attached to the dorsal fin of a shark, the shark's position and heading accuracy are greatly improved as compared to tracking with traditional acoustic tags. The addition of path planning into a provably stable distributed AUV circumnavigation control system allows for collision avoidance with stationary obstacles and a reduction in the interference with fish behavior. Many hours of deployments in California coastal areas validate these claims in system performance.

Future work for this project includes increasing the tracking of multiple tagged individuals, or even populations of fish. New algorithms for multi-AUV/multi-target tracking and cooperative target state estimation. As well, the system will be tested with a variety of different fish species, including sharks, stingrays, bass, and wrasses that exhibit different motion behavior patterns.

ACKNOWLEDGMENTS

REFERENCES

Clark, C. M., Forney, C., Manii, E., Shinzaki, D., Gage, C., Farris, M., Lowe, C. G., & Moline, M. (2013). Tracking and following a tagged leopard shark with an autonomous underwater vehicle. Journal of Field Robotics, 30(3), 309–322.

Espinoza, M., Farrugia, T. J., Webber, D. M., Smith, F., & Lowe, C. G. (2011). Testing a new acoustic telemetry technique to quantify long-term fine-scale movements of aquatic animals. Fisheries Research, 108, 364–371.

Forney, C., Manii, E., Farris, M., Moline, M., Lowe, C. G., & Clark, C. M. (2012). Tracking of a tagged leopard shark with an AUV: Sensor calibration and state estimation. In Proceedings of the 4th International Conference on Robotics and Automation.

Freitag, L., Grund, M., Singh, S., Partan, J., Koski, P., & Ball, K. (2005). The WHOI micro-modem: An acoustic communications and navigation system for multiple platforms. In OCEANS, 2005. Proceedings of MTS/IEEE.

Georgiades, C., German, A., Hogue, A., Liu, H., Prahacs, C., Ripsman, A., Sim, R., Torres, L., Zhang, P., Buehler, M. et al. (2004). Aqua: An aquatic walking robot. In Intelligent Robots and Systems, 2004.(IROS 2004). Proceedings. 2004 IEEE/RSJ International Conference on (Vol. 4, pp. 3525–3531). Sendai, Japan.

Grothues, T., Dobarro, J., & Eiler, J. (2010). Collecting, interpreting, and merging fish telemetry data from an AUV: Remote sensing from an already remote platform. In Autonomous Underwater Vehicles (AUV), 2010 IEEE/OES (p. 1–9). Monterey, CA.

Grothues, T. M., Dobarro, J., Ladd, J., Higgs, A., Niezgoda, G., & Miller, D. (2008). Use of a multi-sensored AUV to telemeter tagged Atlantic sturgeon and map their spawning habitat in the Hudson river, USA. In Autonomous Underwater Vehicles, 2008. AUV 2008. IEEE/OES (pp. 1–7). Woods Hole, MA.

Hart, P. E., Nilsson, N. J., & Raphael, B. (1968). A formal basis for the heuristic determination of minimum cost paths. IEEE Transactions on Systems Science and Cybernetics, 4(2), 100–107.

Haulsee, D. E., Breece, M. W., Miller, D. C., Wetherbee, B. M., Fox, D. A., & Oliver, M. J. (2015). Habitat selection of a coastal shark species estimated from an autonomous underwater vehicle. Marine Ecology Progress Series, 528, 277–288.

Hight, B. V., & Lowe, C. G. (2007). Elevated body temperatures of adult female leopard sharks, *Triakis semifasciata*, while aggregating in shallow nearshore embayments: Evidence for behavioral thermoregulation?

Journal of Experimental Marine Biology and Ecology, 352, 114–128.

Kobilarov, M., Sukhatme, G., Hyams, J., & Batavia, P. (2006). People tracking and following with mobile robot using an omnidirectional camera and a laser. In Proceedings of the 2006 IEEE International Conference on Robotics and Automation.

Latombe, J.-C. (1991). Robot motion planning. Norwell, MA: Kluwer Academic.

LaValle, S. M. (2006). Planning algorithms. New York, NY: Cambridge University Press.

Lin, Y., Kastein, H., Peterson, T., White, C., Lowe, C. G., & Clark, C. M. (2013). Using time of flight distance calculations for tagged shark localization with an AUV. In Proceedings of the Unmanned Untethered Submersible Technology Conference.

Lin, Y., Kastein, H., Peterson, T., White, C., Lowe, C. G., & Clark, C. M. (2014). A multi-AUV state estimator for determining the 3D position of tagged fish. In Intelligent Robots and Systems (IROS 2014), 2014 IEEE/RSJ International Conference on (pp. 3469–3475).

Lowe, C. G., & Bray, R. N. (2006). Fish movement and activity patterns. In The Ecology of California Marine Fishes (pp. 524–553). Berkeley: University of California Press.

Montemerlo, M., Thrun, S., & Whittaker, W. (2002). Conditional particle filters for simultaneous mobile robot localization and people-tracking. In Proceedings of the 2002 IEEE International Conference on Robotics and Automation (Vol. 1, pp. 695–701).

Noda, T., Kawabata, Y., Arai, N., Mitamura, H., & Watanabe, S. (2014). Animal-mounted gyroscope/accelerometer/magnetometer: In situ measurement of the movement performance of fast-start behaviour in fish. Journal of Experimental Marine Biology and Ecology, 451, 55–68.

Oliver, M. J., Breece, M. W., Fox, D. A., Haulsee, D. E., Kohut, J. T., Manderson, J., & Savoy, T. (2013). Shrinking the haystack: Using an AUV in an integrated ocean observatory to map Atlantic sturgeon in the coastal ocean. Fisheries, 38, 210–216.

Packard, G. E., Kukulya, A., Austin, T., Dennett, M., Littlefield, R., Packard, G., Purcell, M., Stokey, R., & Skomal, G. (2013). Continuous autonomous tracking and imaging of white sharks and basking sharks using a REMUS-100 AUV. In Oceans 2013 (San Diego).

Rife, J., & Rock, S. M. (2003). Segmentation methods for visual tracking of deep-ocean jellyfish using a conventional camera. IEEE Journal of Ocean Engineering, 28, 595–608.

Scharold, J., Lai, N. C., Lowell, W. R., & Graham, J. B. (1989). Metabolic rate, heart rate, and tailbeat frequency during sustained swimming in the leopard shark triakis semifasciata. Experimental Biology, 48, 223–230.

Schulz, D., Burgard, W., Fox, D., & Cramers, A. (2001). Tracking multiple moving objects with a mobile robot. In Computer Vision and Pattern Recognition, IEEE Computer Society Conference.

Schulz, D., Burgard, W., Fox, D., & Cremers, A. (2003). People tracking with mobile robots using sample-based joint probabilistic data association filters. International Journal of Robotics Research, 22(2), 99–116.

Shepard, E. L. C., Wilson, R. P., Quintana, F., Laich, A. G., Liebsch, N., Albareda, D. A., Halsey, L. G., Gleiss, A., Morgan, D. T., Myers, A. E., Newman, C., & Macdonald, D. W. (2008). Identification of animal movement patterns using tri-axial accelerometry. Endangered Species Research, 10, 47–60.

Tang, S., Shinzaki, D., Lowe, C. G., & Clark, C. M. (2012). Multi-robot control for circumnavigation of particle distributions. In Proceedings of the International Symposium on Distributed Autonomous Robot Systems.

Thrun, S. (2002). Particle filters in robotics. In Proceedings of the 17th Annual Conference on Uncertainty in AI (UAI) (Vol. 1).

Thrun, S., Burgard, W., & Fox, D. (2005). Probabilistic robotics. Cambridge, MA: MIT Press.

Zhou, J., & Clark, C. M. (2006). Autonomous fish tracking by ROV using monocular camera. Computer and Robot Vision, Canadian Conference, 0, 68.